LWT - Food Science and Technology 189 (2023) 115472

Contents lists available at ScienceDirect

LWT

journal homepage: www.elsevier.com/locate/lwt

Model-based investigation of water adsorption in Achira (*Canna edulis* K.) biscuits

Gentil A. Collazos-Escobar [a], Nelson Gutiérrez-Guzmán [b], Henry A. Váquiro-Herrera [c], José Bon [a], Juan A. Cárcel [a], José V. García-Pérez [a,*]

[a] Grupo de Análisis y Simulación de Procesos Agroalimentarios (ASPA), Instituto Universitario de Ingeniería de Alimentos–FoodUPV, Universitat Politécnica de València, Camí de Vera s/n, Edificio 3F, 46022, Valencia, Spain
[b] Centro Surcolombiano de Investigación en Café CESURCAFÉ, Universidad Surcolombiana, Neiva-Huila, Colombia
[c] Facultad de Ingeniería Agronómica, Universidad del Tolima, Ibagué-Tolima, Colombia

ARTICLE INFO

Keywords:
Hygroscopicity
Monolayer moisture content
Spontaneity
Integral entropy
Machine learning

ABSTRACT

The water adsorption properties of Achira biscuits were investigated using a mathematical model-based strategy to understand the relationship between water activity and moisture content due to the fact that it is highly relevant for its storage. For this purpose, the water adsorption isotherms of commercial Achira biscuits were firstly experimentally determined by the dynamic dew point (DDI) method at 25, 35, and 45 °C and ATR–FTIR spectroscopy was used to detect the functional groups. Secondly, the Guggenheim-Anderson-de Boer (GAB) equation, 4 empirical models (Smith, Oswin, Peleg and DLP), and 5 machine-learning techniques (Regression trees, Random Forest, k-Nearest Neighbors, Artificial Neural Networks and Support Vector Machine) were used to model the isotherms. The fundamentals of water adsorption were analyzed via GAB model parameters, adsorption surface area, spreading pressure, effective pore size, and thermodynamic properties, such as enthalpy-entropy and Gibbs free energy. The experimental results reflected a type III water isotherm and a moderate temperature effect. The GAB model quantified the effect of temperature on the adsorption properties, which reflected a lower degree of hygroscopicity at high temperatures. The Support Vector Machine Learning model provided the best mathematical description of the water adsorption isotherms considering the temperature effect (MRE<3% and R^2_{adj}>99%).

1. Introduction

Mathematical modeling is a powerful tool for investigating and understanding complex manufacturing processes. Computer mathematical modeling enables the description, prediction and optimization of the process behavior for the purposes of improved decision-making at real-time (Kademi et al., 2019). In this way, a mathematical model-based investigation may bring multiple advantages, including improved food safety and quality, reduced costs, increased process efficiency, and a deeper understanding of the underlying process mechanisms. However, it is important to note that the use of a model-based investigation is dependent on the quality and accuracy of the experimental data used to create the model (Schmitt et al., 2020).

During storage, the monitoring and control of both the temperature and relative humidity (%RH) are essential (Tripetch & Borompichaichartkul, 2019). Among other things that may be seriously affected by ignorance of these variables are the textural properties of foodstuffs, which would promote quality losses (Wang et al., 2021). Water sorption isotherms represent the relationship between the food moisture content and water activity (Alyousef et al., 2020). In this sense, at equilibrium, the water activity is equal to the room's relative humidity. Thereby, water adsorption or desorption occurs spontaneously if the product is exposed to a relative humidity that is higher or lower than its water activity, respectively. By the accurate mathematical modeling of experimental water sorption isotherms, the effective surface area, spreading pressure and pore radius can be precisely estimated, as can the thermodynamic adsorption properties, such as differential and integral enthalpy/entropy and Gibbs free energy, (Tao et al., 2018). These properties play an important role in understanding the interactions and mechanisms in the water-binding process and constitute reliable criteria for predicting the storage stability of dehydrated food products.

Traditionally, experimental sorption isotherms have been

* Corresponding author.
E-mail addresses: gencoles@etsiamn.upv.es (G.A. Collazos-Escobar), jogarpe4@tal.upv.es (J.V. García-Pérez).

https://doi.org/10.1016/j.lwt.2023.115472
Received 5 May 2023; Received in revised form 21 September 2023; Accepted 27 October 2023
Available online 28 October 2023

experimentally obtained via the saturated salt slurries method. However, this is a time-consuming technique due to the length of time that samples need to reach equilibrium, which also promotes microbial alterations affecting the structural and compositional properties (Schmidt and Lee, 2012). Of the different alternatives, the high-precision Dynamic Dewpoint Isotherm (DDI) provides high speed analysis and increases the number of sorption data acquired (Romani et al., 2016), which is essential for a subsequent robust computer modeling (Aouaini et al., 2015). Previous studies evaluated the reliability of a model-based investigation for the successful quantification of water sorption properties using DDI analysis in dehydrated and/or baked food products (Romani et al., 2016; Iaccheri et al., 2015; Collazos-Escobar et al., 2020; Carter et al., 2015; Cristina Duarte Marques et al., 2020).

Considering the high degree of complexity and variability of food matrices and the large volume of experimental data provided by the DDI method, investigation into mathematical models with which to describe water sorption isotherms for a particular product is a matter of relevant research (Bon et al., 2012). In this framework, theoretical (Brunauer--Emmett-Teller-BET and Guggenheim-Anderson-de Boer-GAB) and data-driven empirical models (Smith, Oswin, Halsey, Henderson, among others) have been proposed for the modeling of the water sorption behavior of materials (Cristina Duarte Marques et al., 2020). Nonetheless, the robustness of machine-learning algorithms, such as Regression Trees (RT), Random Forest (RF), k-Nearest Neighbors (kNN), Artificial Neural Networks (ANN), and Support Vector Machine (SVM) could also be applied to address the computer modeling of water adsorption isotherms due to their ability to describe non-linear trends (Velásquez et al., 2021). These techniques have been applied in multivariate analyses in order to manage a large number of input variables in many different food manufacturing processes (Tanui et al., 2022).

Achira biscuits are made from a mixture of Achira starch and other non-farinaceous ingredients. During manufacturing (mixing, former and baking processes), standardized processing is crucial to ensure freshness and meet the growing international demand. In this sense, water adsorption analysis is essential in order to address the shelf-life of Achira biscuits due to its impact on the textural attributes during storage. As a bakery product, the analysis of the water adsorption properties of Achira biscuits is essential to understand not only the mechanism involved but also the interaction between the water molecules and the solid matrix. Achira biscuits are considered a low-moisture product; thus, a slight increase in their moisture content may have a great impact on the quality attributes, shortening the shelf-life.

Due to the lack of literature regarding the water adsorption properties of Achira biscuits, this work aims: (i) to experimentally determine the water adsorption isotherms of Achira biscuits at 25, 35, and 45 °C using the DDI method, (ii) to analyze both water adsorption properties and differential/integral thermodynamic properties via the GAB model and (iii) to address the computer modeling of the water adsorption isotherms using GAB, empirical equations and machine-learning techniques to describe the influence of the a_w and temperature on the equilibrium moisture content.

2. Materials and methods

2.1. Raw material

Artisan Achira biscuit samples were purchased in a local store in Neiva (Huila region, Colombia). The samples used for laboratory analysis were manufactured on August 15, 2019 and purchased on August 16, 2019. The expiration date of this batch was November 15, 2019. According to the manufacturer, the Achira biscuits were manufactured using Achira starch (270 g, 30.86% w/w), fresh cheese (500 g, 57.15% w/w), butter (50 g, 5.71% w/w), eggs (50 g, 5.71% w/w) and salt (5 g, 0.57%). Firstly, all the components were mechanically mixed and the biscuits were cut into shapes by hand. Subsequently, the Achira biscuits were baked at 200 °C for 20 min. Finally, the biscuits were tempered for 2 h at room conditions (25 °C and 40% RH) and packaged in polypropylene bags (250 g).

2.1.1. Physicochemical properties

The moisture content of Achira biscuits was determined in triplicate by drying 10 g milled samples in an oven (UF55, Memmert GmbH + Co. KG, Schwabach, Germany) at 105 °C until constant weight (24 h approximately). The results are expressed as a percentage of dry basis (% d.b.). The a_w was measured in triplicate using a vapor sorption analyzer (VSA Aqualab Decagon Devices, Inc. Pullman, WA). 4.0 g of milled samples were used in each trial. The color assessment was performed in triplicate with a spectrocolorimeter (CR−410, Konica Minolta, NJ, USA), considering standard light source D65 and standard observer 10°. A standard white plate was used to calibrate the instrument (Y = 87.0, x = 0.3160, y = 0.3231). The results were expressed according to the CieLab color system (L: lightness, a: redness, and b: greenness). From the color coordinates, the hue angle (h) and chroma or saturation (C_r) were obtained by Eq. (1) and Eq. (2), respectively.

$$h = \text{arctg}\left(\frac{b}{a}\right) \tag{1}$$

$$C_r = \left(a^2 + b^2\right)^{0.5} \tag{2}$$

The mechanical behavior of the Achira biscuit samples was determined at 25 ± 2 °C using a Texture Analyzer (CT3, Brookfield Engineering Laboratories, Canada). A shear blade (TA−52, Brookfield Engineering Laboratories, Canada) was used to carry out the compression tests, applying a deformation of 20% at a rate of 0.5 mm s^{-1} (Ramírez et al., 2016). The measurements were taken in triplicate and the fracture force (F_r, N) was computed.

2.1.2. Fourier-transform infrared (FTIR) spectroscopy

Mid-infrared (MIR) spectral information was obtained using an FTIR spectrophotometer (Cary 630, Agilent Technologies, Santa Clara, CA) coupled with a horizontal ATR sampling accessory (Diamond ATR) equipped with a ZnSe cell. The infrared spectra were obtained in the 4000–650 cm^{-1}wavenumber range, using 8 cm^{-1} resolution, a scan rate of 20, and background correction. Additionally, all of the spectra were preprocessed with a baseline correction using the *ChemoSpec* (Hanson, 2023) function of the statistical software R Core Team (2023) to compensate for any bias in the experimental conditions (Collazos-Escobar et al., 2022).

2.2. Water adsorption analysis

2.2.1. Experimental adsorption isotherms

The experimental water adsorption isotherms of Achira biscuits were determined by means of the dynamic dewpoint isotherm (DDI) method, employing a VSA (Aqualab Decagon Devices, Inc. Pullman, WA) instrument. In every test, 3–3.5 g of Achira biscuits were used and adsorption isotherms were obtained in triplicate at 25, 35, and 45 °C, over an a_w range of 0.1–0.8 with intervals of 0.01 a_w and under an airflow of 100 mL min^{-1} (Collazos-Escobar et al., 2022).

2.2.2. GAB model fitting and related adsorption properties

In order to estimate the water adsorption properties of Achira biscuits, the GAB model (Eq. (3)) parameters were identified at each experimental temperature. For this purpose, the GAB model (Eq. (3)) was arranged as a two-order polynomial (Eq. (4)) and fitted to the experimental data. Thereby, the monolayer equilibrium moisture content (X_m,% d.b.), C and K model parameters were identified by minimizing the mean square error (MSE, Eq. (5)) using the generalized reduced gradient (GRG) optimization method Solver tool available in the Excel spreadsheet (Microsoft) (Sánchez-Torres et al., 2021).

$$X_e = \frac{X_m\, CKa_w}{(1 - Ka_w)(1 + (C - 1)Ka_w)} \tag{3}$$

$$\frac{a_w}{X_e} = \frac{1}{X_m C\, K} + \frac{C - 2}{X_m C} a_w + \frac{K(1 - C)}{X_m C} a_w^2 \tag{4}$$

$$MSE = \frac{\sum_{i=1}^{N} \left(Y_{exp} - Y_{pred}\right)^2}{N} \tag{5}$$

Where X_e is the equilibrium moisture content (% d.b.), Y_{exp} and Y_{pred} are the experimental and predicted responses (a_w/X_e), respectively, and N is the number of experimental data.

In order to assess the influence of temperature on the C and K parameters and estimate the water sorption heats of the monolayer (H_m) and multilayer (H_n) (kJ mol^{-1}), an Arrhenius-type relationship is considered, as illustrated in Eq. (6) and Eq. (7):

$$C = C_0 \exp\left(\frac{H_m - H_n}{RT}\right) \tag{6}$$

$$K = K_0 \exp\left(\frac{L_r - H_n}{RT}\right) \tag{7}$$

where K_0 and C_0 are preexponential (GAB) parameters, R is the universal gas constant of water vapor (8.31447 × 10^{-3} kJ mol^{-1} K^{-1}), L_r is the latent heat of water vaporization (kJ mol^{-1}) and T is the temperature (K).

From the monolayer moisture content, the C and K GAB parameters, the adsorption surface area (m^2 g^{-1} dry basis) and the spreading pressure (J m^{-2}) of Achira biscuits were computed at different temperatures, using Eq. (8) and Eq. (9), respectively:

$$S_A = X_m \left(\frac{1}{M_w}\right) N_0 A_m \tag{8}$$

$$\pi = \frac{kT}{A_m} \ln\left[\frac{1 + CKa_w - Ka_w}{1 - Ka_w}\right]_{0.05}^{a_w} \tag{9}$$

where M_w is the molecular weight of water (kg mol^{-1}), N_0 is the Avogadro number (6 × 10^{23} molecules mol^{-1}), A_m is the area for a water molecule (1.06 × 10^{-19} m^2 molecule^{-1}), and k is Boltzmann's constant (1.380 × 10^{-23} J K^{-1}) (Červenka et al., 2019).

The critical pore size (r_c, nm) was estimated using the Kelvin equation (Eq. 10) and the Halsey expression (Eq. 11) was used to obtain the adsorbed water multilayer thickness (t, nm) (Tao et al., 2018). Thus, the effective pore size (r_p, nm) of adsorption can be computed using Eq. (12).

$$r_c = -\frac{2\sigma V_m}{RT \ln(a_w)} \tag{10}$$

$$t = 0.354\left(\frac{-5}{\ln(a_w)}\right)^{1/3} \tag{11}$$

$$r_p = r_c + t \tag{12}$$

where σ is the surface tension of water (N m^{-1}) and V_m is the molar of adsorbate in a bulk liquid state (m^3 mol^{-1}).

2.2.3. Thermodynamic properties

The thermodynamic analysis of water adsorption in Achira biscuits was computed from differential and integral analyses of isotherms at different temperatures. Thereby, Gibbs free energy, differential/integral enthalpy and entropy were assessed, as explained below.

2.2.3.1. Differential properties. Gibbs free energy for water adsorption (ΔG), was computed using Eq. (13).

$$\Delta G = RT \ln(a_w) \tag{13}$$

The net isosteric heat of adsorption or differential enthalpy of adsorption (ΔH_{diff}) was calculated by the Clausius-Clapeyron equation (Eq. 14), employing a graphical method according to Sánchez-Torres et al. (2021). Meanwhile, the differential adsorption entropy (ΔS_{diff}) was computed via the difference between ΔH_{diff} and ΔG at the different temperatures (Eq. (15)).

$$\Delta H_{diff} = -R\left[\frac{\partial(\ln a_w)}{\partial\left(\frac{1}{T}\right)}\right]_{X_e} \tag{14}$$

$$\Delta S_{diff} = -\frac{\Delta H_{diff} - \Delta G}{T} \tag{15}$$

The linear relationship between differential enthalpy–entropy was the criterion used to assume the compensation theory (Červenka et al., 2019). Eq. (16):

$$\Delta H_{diff} = T_\beta \Delta S_{diff} + \Delta G_\beta \tag{16}$$

where T_β is the isokinetic temperature (K), and ΔG_β is the Gibbs free energy at the isokinetic temperature. If T_β is different from the harmonic temperature (T_{hm}), the compensation theory is valid. The harmonic temperature was computed by Eq. (17).

$$T_{hm} = \frac{n_t}{\sum_{i=1}^{n_t}\left(\frac{1}{T_i}\right)} \tag{17}$$

where n_t is the total number of isotherms.

2.2.3.2. Integral properties. The integral properties were calculated according to Červenka et al. (2019). The net integral heat (integral enthalpy) of adsorption (ΔH_{int}), can be calculated in a similar way to differential enthalpy (Eq. (14)), maintaining the spreading pressure constant, as observed in Eq. (18).

$$\Delta H_{int} = -R\left[\frac{\partial(\ln a_w)}{\partial\left(\frac{1}{T}\right)}\right]_{\pi} \tag{18}$$

Additionally, changes in the integral entropy (ΔS_{int}) were calculated using Eq. (19):

$$\Delta S_{int} = -\frac{\Delta H_{int} - R\ln(a_w)^*}{T} \tag{19}$$

where $(a_w)^*$ was the geometric water activity interpolated at a constant spreading pressure for every experimental temperature.

2.3. Mathematical modeling of water adsorption isotherms

The mathematical modeling of the water adsorption isotherms of Achira biscuits was addressed by using i) a classical approach from the GAB and empirical equations and ii) machine-learning algorithms. Both approaches were used not only to describe the changes in water adsorption isotherms considering the effect of temperature but also to obtain a robust model with which to perform an accurate prediction of the equilibrium moisture content of this product during storage.

2.3.1. Classical approach modeling

The theoretical GAB model (Eq. (3)) was fitted to the experimental data of the water adsorption isotherms of Achira biscuits, as described in section 2.2.2. Moreover, empirical equations, such as Smith's, Oswin's, Peleg's, and the DLP (Table 1, Eq. 20 to 23), were also tested. These models were initially adjusted at each experimental temperature,

Table 1
Mathematical models used to describe the water adsorption isotherms of Achira biscuits.

Model	Mathematical expression	Reference	Eq. No
Smith	$X_e = b_1 - b_2 \ln(1 - a_w)$	Arslan-Tontul (2020)	20
Oswin	$X_e = b_1 \left(\frac{a_w}{1 - a_w}\right)^{b_2}$	Monte et al. (2018)	21
Peleg	$X_e = b_0 {a_w}^{b_1} + b_2 {a_w}^{b_3}$	Arslan-Tontul (2020)	22
DLP	$X_e = b_0 + b_1 x + b_2 x^2 + b_3 x^3\ x = \ln(-\ln a_w)$	Yogendrarajah et al. (2015)	23

wherein their unknown parameters (b_i) were identified using a Genetic Algorithm ("ga", MATLAB function) and then linearly linked with temperature according to Collazos-Escobar et al. (2020). Afterward, the b_i parameters found were optimized using the "nlinfit" function, and their confidence intervals (95%) were determined via the "nlparci" function. The non-linear Ordinary Least Square (OLS) regression procedures and statistical parameter estimation was carried out using MATLAB® R2023a (The MathWorks Inc., Natick, MA, USA).

2.3.2. Modeling using machine-learning techniques

Five machine-learning techniques (RT, RF, kNN, ANN and SVM) were also considered for the purposes of mathematically describing the water adsorption isotherms of Achira biscuits. Independent multilevel factorial designs (DOEs) were formulated to optimize the hyperparameters belonging to each machine-learning technique. In this sense, RT was assessed via a DOE (3^1), considering the post-pruning standard error (SE) at three different levels (0.1, 0.5, and 1) as the main factor. As for RF calculations, a DOE (3^2) was set up considering different numbers of trees (100, 550, and 1000) and a square number of inputs (*mtry*), ranging from 2 to 4. The kNN optimization was performed considering a DOE (8^1), wherein a Fast Nearest Neighbor was applied using different numbers of nearest neighbors (2, 3, 4, 8, 12, 16, 20, and 30). ANN architectures were computed via a DOE ($15^1 2^2$), considering a different number of neurons in the hidden layer (one layer with 6–20 neurons), two activation functions (hyperbolic tangent and soft plus), and two resilient backpropagation algorithms (with and without weight backtracking). In a SVM algorithm, a DOE ($2^1 3^2$) was formulated using two kernel functions (*rbfdot* and *laplacedot*), three types (*esp-bsvr*, *esp-svr*, and *nu-svr*) and C (1, 500.5, and 1000).

Computing modeling was carried out using the statistical software, R Core Team (2023), wherein different R-packages were used: the *DMwR2* for RT (Torgo, 2016), the *randomForest* for RF (Liaw & Wiener, 2002), the *FNN* for kNN (Beygelzimer et al., 2023), the *neuralnet* for ANN (Fritsch et al., 2019), and the *kernlab* for SVM (Karatzoglou et al., 2023, pp. 9–32).

2.4. Model training and statistical validation

The experimental data were randomly split 100 times into two data sets: 75% for training and the remaining 25% for model validation (Sanchez-Jimenez et al., 2023). In each iteration, the aforementioned optimization strategy of empirical/machine-learning models was solved, and then trained models were externally validated using the 25% data set. The goodness of fit of the adjusted GAB model at each temperature (section 2.2.2) and the trained/validated models (section 2.3) were evaluated via the adjusted coefficient of determination (R^2_{adj}) (Eq. (25)) and the mean relative error (MRE%) (Eq. (26)):

$$R^2(\%) = 100 - \frac{\sum_{i=1}^{N} \left(Y_{exp} - Y_{pred}\right)^2}{\sum_{i=1}^{N} \left(\overline{Y_{exp}} - Y_{pred}\right)^2} \quad (24)$$

$$R^2_{adj}(\%) = 100 - \left(\frac{N-1}{N-M}\right)\left(100 - R^2\right) \quad (25)$$

$$MRE\ (\%) = \frac{100}{N} \sum_{i=1}^{N} \frac{\left|Y_{exp} - Y_{pred}\right|}{Y_{exp}} \quad (26)$$

where M is the number of model parameters and R^2 is the coefficient of determination between the experimental and predicted values. Figures of MRE<10% and R^2_{adj}>98% reflect a reasonably satisfactory fitting (Silva et al., 2021).

The GAB model parameters and S_A values identified at 25, 35 and 45 °C were processed using the one-way analysis of variance (ANOVA) in order to analyze the significance of the influence of temperature and the means were compared by Fisher's Least Significant Difference (LSD) intervals.

The hyperparameters of machine-learning techniques were optimized using a multifactor ANOVA applied on DOEs (section 2.3.2), wherein a mean pairwise comparison with LSD was used to determine the best algorithm combination for the maximization R^2_{adj} (%) and minimization of MRE (%). Furthermore, to select the best trained model for the purposes of faithfully describing the experimental validation data set (25%), a multifactorial ANOVA was performed considering the models and the partitions of the data set as factors and both R^2_{adj} (%) and MRE (%) as responses to be maximized and minimized, respectively. As in the case of a one-way ANOVA, the means were compared using LSD intervals. Finally, normality (Shapiro-Wilk's test and q-q plot), independence (Ljung-Box's test) and homoscedasticity (Levene's test and multiple linear regression-MLR on square residuals) hypotheses (Cristina Duarte Marques et al., 2020) were assessed in order to analyze the residuals of trained/validated and ANOVA models. Hypothesis tests and statistical assumptions were verified with a 95% confidence level in the abovementioned statistical analysis, which was carried out using STATGRAPHICS Centurion XVIII (Manugistics, Inc., Rockville MD, USA).

3. Results and discussion

3.1. Physicochemical characterization of Achira biscuits

The Achira biscuits (Fig. 1A) presented an initial moisture content and water activity of 2.03 ± 0.16 % d.b. and 0.16 ± 0.02, respectively; thus, they may be considered as low-moisture food (a_w < 0.85) (Acuff et al., 2023). These figures were similar to those reported by Ramírez et al. (2016) for the Achira biscuits: a moisture content of 2.45 ± 0.10 % d.b. and water activity of 0.14 ± 0.03. Similarly, the fracture force (24.4 ± 2.3 N) and the optical properties observed for the Achira biscuits (L* = 63.3 ± 0.6, a* = 4.6 ± 0.4, b* = 27.7 ± 0.7, h = 1.41 ± 0.02 and C_r = 28.1 ± 0.7) were in the range of those found by Ramírez et al. (2016).

The ATR–FTIR spectroscopy technique was used to detect the functional groups available on food adsorption surfaces and their relationship with its constituents (Anastopoulos et al., 2017). In this way, Fig. 2 depicts the average ATR–FTIR infrared spectra of the Achira biscuits at a wavenumber of 4000–650 cm^{-1}. The FTIR spectra (Fig. 2) exhibited high intensities at wavenumbers of 3285 cm^{-1}, 2920 cm^{-1}, 2853 cm^{-1}, 1742 cm^{-1}, 1654 cm^{-1}, 1459 cm^{-1}, 1151 cm^{-1}, 1079 $cm^{-1}$and 991 cm^{-1}. These peaks led to there being two different spectral regions: (i) functional group (3650–1500 cm^{-1}) and (ii) fingerprint (1500–650 cm^{-1}); these are mainly associated with the typical vibration pattern of proteins, lipids, and carbohydrates (Durak & Depciuch, 2020). Due to the lack of any previous literature on Achira biscuits, the FTIR spectra were compared to those reported for Achira starch and to other cereal-based baked products. When analyzing Achira starch, Mendez-Montealvo et al. (2022) observed intensities from 1400 to 1200 cm^{-1} and the absorption band at 2920 cm^{-1}: these are linked to the hydrogen bonding and the asymmetrical deformation (CH_2 twisting), and bands at

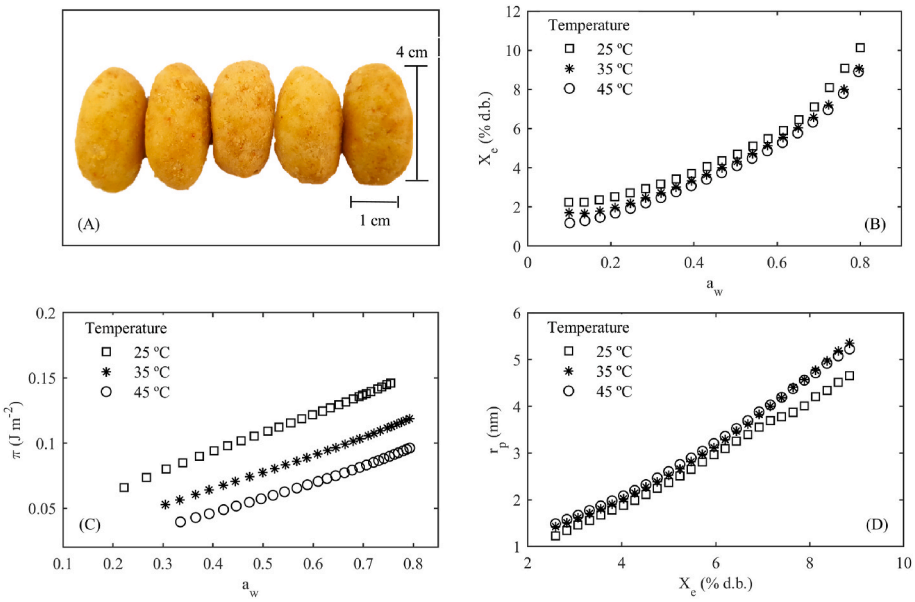

Fig. 1. Achira biscuits (A), experimental average water adsorption isotherms (B), spreading pressure (C), and effective pore size of adsorption (D) at 25, 35, and 45 °C.

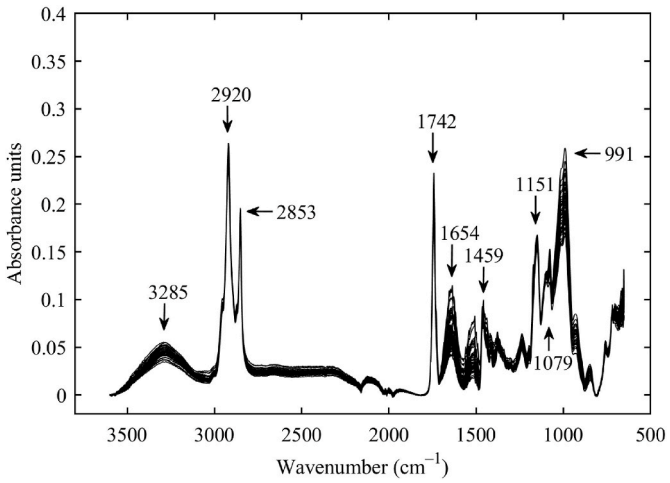

Fig. 2. Average ATR–FTIR spectra of Achira biscuits.

1079 cm^{-1} and 991 cm^{-1} are sensitive to structural changes. These results were quite similar to the present spectral behavior (Fig. 2) due to starch being the main constituent of Achira biscuits (section 2.1). Analyzing rice-oat and maize-oat flours, Ying et al. (2017) reported absorbance peaks at 1700–1600 cm^{-1} and 1570–1534 cm^{-1}, as a result of protein interactions, and at 1200–900 cm^{-1}, which is linked to carbohydrates. Achira biscuits may contain a higher amount of carbohydrates than the flours analyzed by Ying et al. (2017) due to the high signal intensity observed at 991 cm^{-1} (de Cássia Sousa Mendes et al., 2021).

FTIR spectroscopy could be used as an additional technique with which to monitor the Achira biscuits during storage due to its feasibility to detect any change in the functional groups associated with food components. Thereby, different studies have tested the potential of the FTIR technique to detect defects in packaged foods (Baskaran & Sathiavelu, 2020) and to monitor the quality characteristics of olive oil during storage (Üçüncüoğlu & Küçük, 2019).

3.2. Water adsorption properties

The water adsorption isotherms of the Achira biscuits at 25, 35 and 45 °C are depicted together in Fig. 1. The mean experimental curves are presented for the three replicates carried out using the DDI method. The error bars were not included due to the limited experimental variability observed (0.09 % d.b.). The adsorption isotherms at different temperatures (Fig. 1B) exhibited a type III upward J-concave shape according to BET classification, which is characteristic of food matrices rich in soluble components (Herman et al., 2018).

As is illustrated in Fig. 1B, the influence of temperature behaved typically in the range of 25–45 °C; that is, at a certain water activity, the lower the temperature, the higher the equilibrium moisture content. As an example, at 0.1 a_w, the equilibrium moisture content was 2.2, 1.7 and 1.2% d.b. at 25, 35 and 45 °C, respectively. Similarly, at 0.5 a_w, the moisture content decreased significantly (4.7, 4.3, 4.1% d.b.) as the temperature increased. This illustrates that Achira biscuits become more hygroscopic as the temperature falls in the surrounding environment. This result can be explained by the fact that the water mobility at high temperatures (greater kinetic energy) was greater, leading to more interactions of the water molecules with the active sites or other water molecules (Hidar et al., 2018). Similar results have been reported in starch-rich products (Al-Muhtaseb et al., 2010; Galla et al., 2017; Kulchan et al., 2010; McMinn et al., 2007; Romani et al., 2016; Wang et al., 2021).

The GAB model was fitted at each experimental temperature to quantify the water adsorption properties and the differential/integral thermodynamic properties of the Achira biscuits, as explained in section 2.2.2. These properties include the effective surface of adsorption, the spreading pressure, and the pore radius, which are suited to the purposes of understanding the hygroscopic interaction of Achira products with their surroundings during storage. In this way, the GAB model enabled a satisfactory description of water adsorption isotherms at the different temperatures, as is manifested by the statistical parameters shown in Table 2 (R^2>99.5% and MRE<2.5%). The Achira biscuits presented an X_m value of 2.58% d.b. at 25 °C, while the figures identified at 35 and 45 °C were slightly higher (2.66 and 2.65% d.b.) than at 25 °C. This denotes that the temperature effect was moderate from 35 to 45 °C.

Furthermore, the computed X_m values were higher than the initial moisture content of the Achira biscuits (2.03 ± 0.16 % d.b). Therefore,

Table 2
GAB model parameters and adsorption surface area of Achira biscuits.

Temperature (°C)	X_m (% d.b.)	C	K	S_A (m^2 g^{-1} d.b.)	MRE (%)	R^2 (%)
25	2.58 ± 0.03[a]	16.7 ± 1.3[a]	0.95 ± 0.01[a]	91.2 ± 1.1[a]	2.4 ± 0.1	99.7 ± 0.1
35	2.66 ± 0.02[a]	7.1 ± 0.6[b]	0.91 ± 0.01[b]	93.3 ± 0.4[a]	2.4 ± 0.2	99.8 ± 0.1
45	2.65 ± 0.04[a]	3.7 ± 1.3[c]	0.90 ± 0.02[b]	93.0 ± 1.5[a]	2.1 ± 0.2	99.9 ± 0.1
p-value	ns	***	**	ns		

Different lowercase letters indicate statistically significant differences (95%) for each response (GAB parameters and S_A) in terms of the temperature. ns: not significant. *p < 0.05. **p < 0.01.***p < 0.001.

the baking time could be shortened at an industrial level in order to minimize the energy cost and improve the productivity without any impact on product stability. X_m computes the moisture content corresponding to the saturation of all the primary adsorption sites by water molecules (Robertson & Lee, 2021).

The increase in temperature leads to greater kinetic energy in the water molecules, which means that a single molecule may interact with more active sites, reducing the number of molecules attached in the monolayer (Tao et al., 2018). As a function of X_m, the computed S_a resulted in 91.2–93 m^2 g^{-1} d.b.

Fig. 1C and D illustrate how an increase in water activity and moisture content also involves an increase in the spreading pressure and pore radius. The fact that the spreading pressure is higher at 25 °C than at 35–45 °C points to the Achira biscuits having less free energy (affinity of water molecules) at the surface of sorption sites at high temperatures, which has also been previously observed (Cheng et al., 2020; Tao et al., 2018; Červenka et al., 2019). The pore radius of the Achira biscuits ranged from 1.2 to 5.4 nm; according to IUPAC (International Union of Pure and Applied Chemistry), which denotes the presence of micropores (pore sizes < 2 nm) and mesopores (diameter range of 2–50 nm), respectively (Monte et al., 2018). These figures are similar to those reported for water caltrop pericarps (1.7–6.2 nm) (Cheng et al., 2020).

As for the GAB parameters linked to sorption heat in the monolayer (C) and multilayer (K) (Iaccheri et al., 2015), the temperature effect was greater than for the monolayer moisture content. Thus, the C parameter decreased significantly ($p < 0.05$) from 16.7 at 25 °C to 3.7 at 45 °C, while K, in the same experimental range, decreased from 0.95 to 0.90. The fact that both C and K decrease as the temperature drops indicates that less energy is required to bind water molecules to active sorption sites in the monolayer and multilayer (Talens et al., 2018). These C and K figures were similar to those reported in the case of mango powder (C = 5.5 at 20 °C to 2.8 at 40 °C, and K = 0.95 at 20 °C to 0.91 at 40 °C) (Cano-Higuita et al., 2013) and whole chia seeds (C = 6.42 at 25 °C to 4.25 at 35 °C, and K = 0.92 at 25 °C to 0.91 at 35 °C) (Arslan-Tontul, 2020).

3.3. Thermodynamic properties

The variation in the differential and integral thermodynamic properties of the Achira biscuits is shown in Fig. 3. The ΔH identified by integral and differential methods decreased as the equilibrium moisture content increased (Fig. 3A). Thus, in the X_e range from 2.5 to 9% d.b, ΔH_{diff} and ΔH_{int} decreased from 16.3 to 2 kJ mol^{-1} and from 39.1 to 25.1 kJ mol^{-1}, respectively. That the ΔH_{int} figures are higher than those of ΔH_{diff} can be explained by the fact that ΔH_{int} computes the energy linked to water-solid binding, while ΔH_{diff} quantifies water-water interaction, which is weaker (Červenka et al., 2019). Similar results have also been reported when analyzing starch-based products, such as oatmeal biscuits (McMinn et al., 2007) and baked Madeira cake (Al-Muhtaseb et al., 2010). As carbohydrates are the main constituent of Achira biscuits, as illustrated by the FTIR spectrum (Fig. 2), this behavior could be associated with water-starch binding, as reported in other bakery products.

Fig. 3B illustrates the average changes in ΔS_{diff} and ΔS_{int} as a function of X_e. Thus, ΔS_{diff} showed that a sharp increase was found from approximately 2.5 to 3 % d.b, which is explained by the reduction in the number of polar sites and their energy as the adsorption monolayer is being completed. From this point onwards, an almost constant increase was found. This highlighted the fact that it is critical to consider water adsorption when storing Achira biscuits. Small deviations from the monolayer moisture will result in expected structural changes, which will affect the biscuits' shelf life. In the case of ΔS_{int}, a progressive increase was reported as the adsorption progressed pointing to a greater disorder of water molecules and, as a consequence, of stability (Tao et al., 2018).

Negative values of the Gibbs free energy, ΔG, reflect the water molecules' affinity to an adsorbent matrix characterized by a spontaneous exothermic process (Cheng et al., 2020). On this basis, it is possible to infer that for the adsorption process of Achira biscuits to

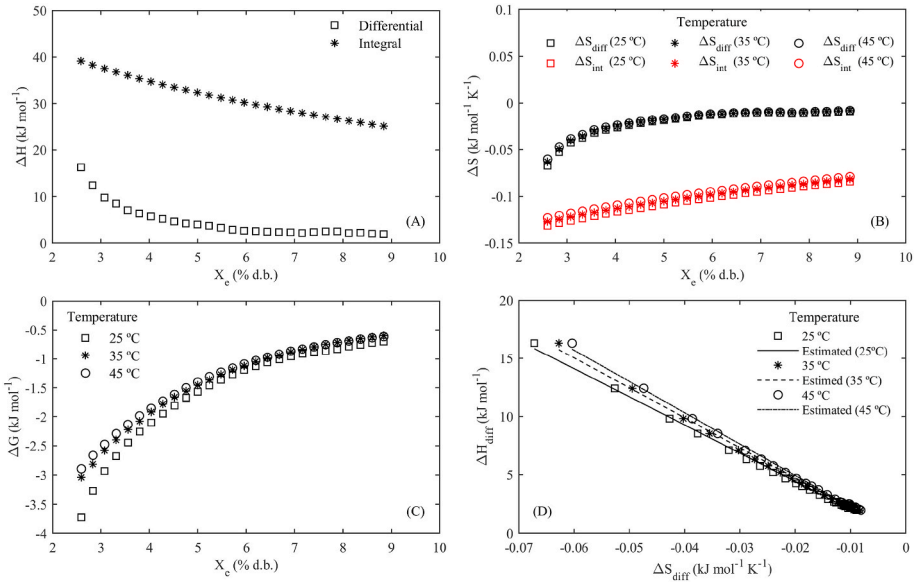

Fig. 3. Differential/integral enthalpy (A), differential/integral entropy (B), Gibbs free energy (C), and compensation theory (D) of Achira biscuits at 25, 35 and 45 °C.

occur, it does not require energy from the surrounding environments. The effect of temperature on ΔG was more marked when the moisture content (Fig. 3C) of Achira biscuits was low. Thus, up to 5% d.b., ΔG at 25 °C was noticeably lower than at 35 and 45 °C, which indicated a greater spontaneity and, therefore, more hygroscopic capacity of the material. These results were similar to those reported in the studies into water caltrop pericarps (Cheng et al., 2020) and black peppercorns (Yogendrarajah et al., 2015).

The differential enthalpy/entropy compensation law at different experimental temperatures was valid, manifested by the linear pattern found between the differential figures of ΔH and ΔS (Fig. 3D). Thus, T_{hm} resulted in 307.9 K and T_{β} values were 241.6 K, 257.6 K, and 268.8 K at the experimental temperatures of 25, 35, and 45 °C, respectively. Due to the fact that T_{hm} (304.9 K) > T_{β}, the validated compensation theory indicates that the adsorption process of Achira biscuits was entropy-driven. In addition, the negative values of ΔG_{β} (y-intercept of the linear fitting) confirmed the spontaneity of the adsorption process, as already illustrated by ΔH (Fig. 3A). Similar results were reported by Viganó et al. (2012) and Silva et al. (2014) when studying low-moisture foodstuffs.

3.4. Mathematical modeling of water adsorption isotherms

The statistical results of the mathematical modeling considering the influence of temperature on water adsorption isotherms are summarized in Table 3. The results are shown separately for the fitting set (using 75% of the experimental data) and their validation (using the remaining 25% of the data). Both R^2_{adj} and MRE were considered as the goodness metrics with which to quantify the ability of the GAB, empirical equations and machine-learning techniques to describe the water adsorption isotherms of the Achira biscuits. In this sense, modeling results reported that the R^2_{adj} values ranged between 99.2% and 99.9% and the MRE from 0.06% to 3.8% for the training data set. These results reflected the noticeable ability of trained GAB and empirical/machine-learning models to represent the dependence of both a_w and temperature on the equilibrium moisture content of the Achira biscuits. In addition to that, the confidence intervals (Table 3) of the trained empirical model parameters were statistically significant (95%), suggesting that their estimation was accurate. Moreover, the optimal configuration of all the trained machine-learning techniques is presented in Table 3; these hyperparameters were statistically significant (95%) and their values provided the best goodness of fit in each trained technique to maximize the predictability of the water adsorption isotherms.

The variation in the parameters of the generalized GAB model (X_m, C_0, K_0, H_m, and H_n) was of a similar magnitude to that found in mango powder by Cano-Higuita et al. (2013), who claimed that the positive relationship between H_m and H_n indicated a strong exothermic interaction of water vapor with primary active sorption sites. This statement is consistent both with the results shown in Fig. 3A regarding the differential enthalpy of adsorption and with those illustrated in Fig. 3C associated with adsorption-spontaneity.

As already explained, the figures of MRE and R^2_{adj} formed the basis for the selection of the best model; thus, the goodness of fit of the trained empirical/machine-learning models can be ordered as follows: SVM > RF > RT > kNN > DLP > ANN > Peleg > Smith > GAB > Oswin. However, it is highly relevant to perform a model residual analysis for their validation before their use for the purposes of predicting the validation data set (25%). Thus, Fig. 4 illustrates both the experimental equilibrium moisture content vs the predicted values via trained models and their residual analysis. A noticeably linear agreement can be observed (Fig. 4) between experimental and predicted values via the GAB (Fig. 4A) and all the empirical/machine-learning models (Fig. 4C, E, 4G, 4I, 4K, 4M, 4O, 4Q, and 4S). Despite this, statistically significant ($p < 0.05$) differences in both non-random patterns (statistically quantified by the Ljung-box test) and heteroscedastic residual behavior (statistically quantified by the Levene test) were observed for the GAB

Table 3
Trained/optimized models (75%) and their statistical results for the validation data set (25%).

Model	Parameters	Confidence intervals (95%)	MRE (%)	R^2_{adj} (%)
GAB	$X_m = 2.8$ (% d. b.) $C_0 = 9.5 \times 10^{6}$ $K_0 = 99.1$ $H_m = 90.3$ kJ mol^{1} $H_n = 55.6$ kJ mol^{1}	[2.7, 2.8] [9.0×10^6, 9.9×10^6] [98.5, 99.7] [90.3, 90.3] [55.6, 55.6]	Training 3.55 ± 0.08 Validation 3.71 ± 0.27^{acA}	Training 99.72 ± 0.01 Validation 99.70 ± 0.02^{aA}
Smith	$b_{1.1} = -3.6 \times 10^4$ K^{1} $b_{1.2} = 0.12$ $b_{2.1} = -4.7 \times 10^5$ K^{1} $b_{2.2} = 0.07$	[-4.0×10^4, -3.3×10^4] [0.11, 0.13] [-9.2×10^5, -1.9×10^6] [−0.05, −0.08]	Training 3.34 ± 0.07 Validation 3.48 ± 0.16^{abA}	Training 99.70 ± 0.01 Validation 99.64 ± 0.03^{bA}
Oswin	$b_{1.1} = -4.2 \times 10^4$ K^{1} $b_{1.2} = 0.17$ $b_{2.1} = 3.7 \times 10^3$ K^{1} $b_{2.2} = -0.6$	[-4.4×10^4, -4.0×10^4] [0.17, 0.18] [3.1×10^3, 4.3×10^3] [−0.8, −0.4]	Training 3.77 ± 0.08 Validation 3.80 ± 0.10^{cA}	Training 99.65 ± 0.02 Validation 99.70 ± 0.02^{bA}
Peleg	$b_{01} = -1.5 \times 10^3$ K^{1} $b_{02} = 0.6$ $b_{11} = 0.1$ K^{1} $b_{12} = -28.4$ $b_{21} = 1.5 \times 10^3$ K^{1} $b_{22} = -0.39$ $b_{31} = 0.03$ K^{1} $b_{32} = -8.4$	[-2.0×10^3, -1.0×10^3] [0.4, 0.7] [0.08, 0.13] [−34.4, −22.3] [1.3×10^3, 1.6×10^3] [−0.45, −0.33] [0.03, 0.03] [−9.1, −7.6]	Training 3.30 ± 0.10 Validation 3.38 ± 0.34^{bA}	Training 99.80 ± 0.01 Validation 99.78 ± 0.02^{cA}
DLP	$b_{01} = -3.4 \times 10^4$ K^{1} $b_{02} = 0.13$ $b_{11} = -1.4 \times 10^4$ K^{1} $b_{12} = 0.02$ $b_{21} = -1.35 \times 10^4$ K^{1} $b_{22} = 0.05$ $b_{31} = 7.7 \times 10^5$ K^{1} $b_{32} = -0.02$	[-3.6×10^4, -3.1×10^4] [0.13, 0.14] [-1.8×10^4, -9.7×10^5] [2.3×10^3, 0.03] [-2.1×10^4, -6.3×10^5] [0.03, 0.07] [1.5×10^5, 1.4×10^4] [−0.04,−4.40 × 10^3]	Training 2.73 ± 0.03 Validation 2.84 ± 0.1^{dA}	Training 99.80 ± 0.01 Validation 99.78 ± 0.02^{cA}
	Optimal configuration			
RT	SE = 0.1		Training 1.53 ± 0.04 Validation 1.90 ± 0.13^{eA}	Training 99.87 ± 0.01 Validation 99.79 ± 0.03^{cA}
RF	Mtry = 4 Number of trees:100		Training 1.28 ± 0.03 Validation 1.57 ± 0.10^{fA}	Training 99.90 ± 0.01 Validation 99.85 ± 0.03^{dA}
kNN	Number of Nearest Neighbors: 2		Training 1.53 ± 0.05 Validation 1.75 ± 0.10^{gA}	Training 99.88 ± 0.01 Validation 99.80 ± 0.03^{cA}
ANN	Neurons: 15 Activation: hyperbolic tangent Algorithm: resilient backpropagation with weight backtracking		Training 3.00 ± 0.10 Validation 2.31 ± 0.10^{hA}	Training 99.23 ± 0.03 Validation 99.30 ± 0.02^{eA}
SVM	Kernel function: laplacedot Type: nu-svr C = 500.5		Training 0.06 ± 0.01 Validation 0.65 ± 0.06^{iA}	Training 99.9 ± 1.1 × 10^{-3} Validation 99.93 ± 0.02^{fA}

Different lowercase letters indicate statistically significant differences (95%) for each goodness of fit metric (R^2_{adj} and MRE) as a function of the GAB, empirical

and machine learning models; uppercase letters indicate statistically significant differences for the training/validation iterations performed. ns: not significant. *p < 0.05. **p < 0.01.***p < 0.001.

(Fig. 4B), Smith (Fig. 4F), RF (Fig. 4H), Oswin (Fig. 4J), Peleg (Fig. 4N), ANN (Fig. 4P) and DLP (Fig. 4R) models; the RT and kNN residuals, meanwhile, were random ($p > 0.05$), but heteroscedastic ($p < 0.05$). Finally, the SVM residuals (Fig. 4T) were random and homoscedastic ($p > 0.05$). According to Cristina Duarte Marques et al. (2020), a failure to satisfy either of the two assumptions concerning the residuals invalidates the model for its use as a predictive tool. In this regard, it was possible to validate only the SVM model for predictive purposes due to its agreement with the aforementioned residual hypotheses.

Although the trained models (except the SVM) were not adequately validated via residual analysis, they were also tested using the validation data set to quantify the ability of these models to predict unknown observations. As already explained in section 2.4, a multifactor ANOVA was used to select the model which best describes the validation data set. Thus, the mean pairwise comparisons based on both R^2_{adj} (%) and MRE (%) evidenced statistically significant differences ($p < 0.05$) via the first factor (type of trained model), whereas the second (random partition of data sets) did not show statistically significant differences ($p > 0.05$). Via the LSD intervals (Table 3), it was possible to order them as follows: SVM > RF > kNN > RT > ANN > DLP > Peleg > Smith > GAB > Oswin. Furthermore, the homogeneous groups defined via the LSD intervals provided a reliable statistical benchmark with which to properly select the best model to maximize R^2_{adj} and minimize MRE. In this way, the SVM model was the most suitable for the purposes of describing the influence of a_w and temperature on the equilibrium moisture content of the Achira biscuits due to its greater goodness of fit (MRE = 0.65 ± 0.06% and R^2_{adj} = 99.9 ± 0.02%), which was confirmed by its independent LSD group. These results highlight SVM as a valuable and reliable tool with which to offer a faithful prediction of the complexity of the experimental data set determined via the DDI method.

The goodness of fit of the SVM and the residual analysis for the validation data set (25%) are illustrated together in Fig. 5. Fig. 5A shows how SVM modeling was used to describe both the type III upward J-concave hygroscopic behavior of the Achira biscuits and the temperature influence on the water adsorption isotherms. A close agreement between the experimental and predicted equilibrium moisture contents (Fig. 5B) was found, indicating that the prediction of the experimental response was quite similar. In addition, the model's residuals for the validation data set (Fig. 5C) exhibited random and homoscedastic ($p > 0.05$) behavior, confirming the feasibility of employing SVM to predict unknown observations faithfully.

Modeling water sorption isotherms in Achira biscuits was primarily an experimental data-driven task. Consequently, exploring various ML models became imperative in order to properly address the experimental variability in the adsorption process. In this context, an in-depth understanding of the mathematical foundations behind each ML technique was essential for the purposes of interpreting the outcomes presented in Table 3.

In the case of RT, the decision criteria were mathematically based on dividing experimental data into RT nodes to optimize the model fitting. In contrast, RF ensembles 100 randomly selected RTs to improve diversity, following the bagging principle, and uses mathematical averaging to avoid overfitting. This approach reduces the sensitivity of the model to variations in the training data (Otchere, 2023) resulting in a more robust approach than the single RT. This aspect is observed in the greater goodness of fit ($p < 0.05$) for the validation dataset in RF (MRE = 1.57 ± 0.10% and R^2_{adj} = 99.85 ± 0.03%) compared to RT (MRE = 1.90 ± 0.13% and R^2_{adj} = 99.79 ± 0.03%).

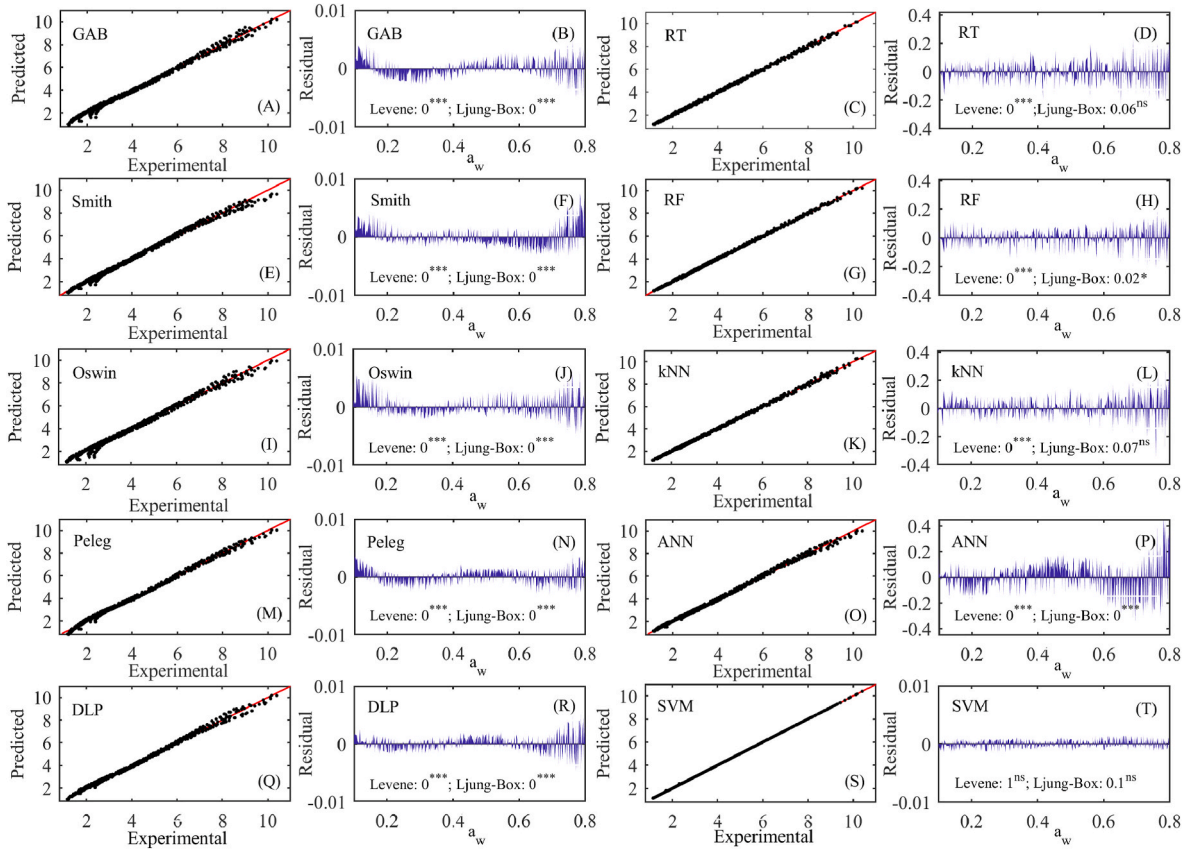

Fig. 4. Experimental equilibrium moisture content vs values predicted via the GAB and empirical/machine learning models and residual analysis for training data set (75%).

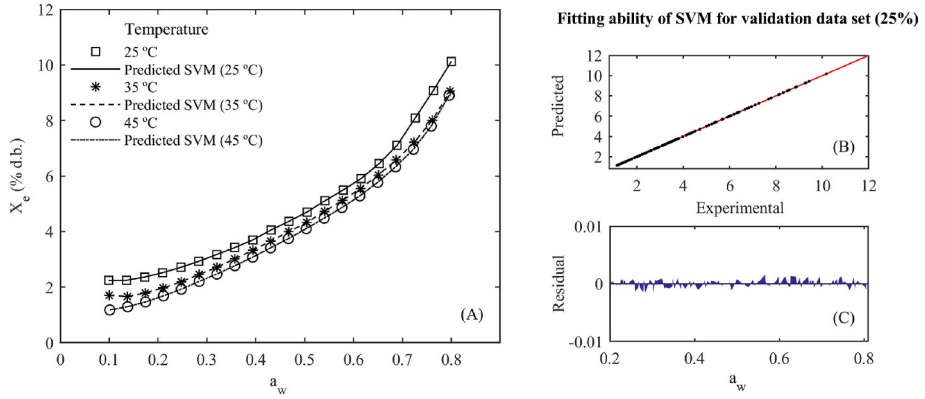

Fig. 5. SVM model for water adsorption isotherms of Achira biscuits at different temperatures (A), experimental equilibrium moisture content values vs values predicted by SVM (B), and SVM residual plot for validation data set (25%) (C).

The estimation of model ANN parameters considers linear algebra for weighted connections and error optimization through backpropagation. In contrast, kNN uses the Euclidean distance and statistical methods based on mathematical proximity for classification and regression tasks. The statistical outcomes of the ANN model (MRE = 2.31 ± 0.10% and R^2_{adj} = 99.30 ± 0.02%) were lower in comparison to RT, RF, kNN (MRE = 1.75 ± 0.10% and R^2_{adj} = 99.80 ± 0.03%). The best accuracy in ML models was achieved by SVM (MRE = 0.65 ± 0.06% and R^2_{adj} = 99.93 ± 0.02%). SVM represents a complex approach from a mathematical point of view, which relies on vector spaces and margin optimization to identify hyperplanes and separate data classes. Thereby, SVM allows for the accurate handling of linear and nonlinear systems by employing kernel functions to transform data into higher-dimensional spaces (Sairamya et al., 2019). Considering the mathematical background of SVM and from its optimal configuration established through a multifactor ANOVA (as detailed in section 2.4 and Table 3), this model emerged as the most suitable choice for the purposes of characterizing the water sorption isotherms of the Achira biscuits. The feasibility of SVM has also been satisfactorily tested in many applications, such as for the discrimination of Extra Virgin Olive Oils (Scatigno & Festa, 2022) and to model the drying process of coffee cherry beans (Velásquez et al., 2021).

4. Conclusions

Model-based investigation strategy was applied for the purposes of analyzing the water adsorption process of Achira biscuits. The fit of the theoretical GAB equation (R^2>99.5% and MRE<2.5%) reflected a moderate role of the temperature on the isotherms, less hygroscopicity at high temperatures and spontaneous and entropy-driven adsorption (T_{hm} = 307.9 K > T_β = 257.6 K). This behavior was well supported by the ATR-FTIR analysis.

Support Vector Machine Model-Based Learning permitted an accurate description of the water adsorption isotherms (MRE<3% and R^2_{adj}>99%), allowing the real-time monitoring of the moisture content of the biscuits as a function of their storage conditions.

This analysis does not consider the inherent variability of commercial Achira biscuits; thus, further studies should address the effect of different formulations of Achira biscuits on the adsorption properties. In addition, computing how sensory and textural attributes are modified by moisture content is essential for storage purposes, as well as its integration into machine-learning algorithms in order to support and improve decision-making on an industrial level. This approach would greatly contribute to the real-time quality control of Achira biscuits.

CRediT authorship contribution statement

Gentil A. Collazos-Escobar: Investigation, Methodology, Formal analysis, Software, Writing – original draft, Writing – review & editing. **Nelson Gutiérrez-Guzmán:** Conceptualization, Investigation, Methodology, Supervision, Writing – review & editing. **Henry A. Váquiro-Herrera:** Conceptualization, Investigation, Methodology, Software, Writing – review & editing. **José Bon:** Methodology, Funding acquisition, Software, Writing – original draft, Writing – review & editing. **Juan A. Cárcel:** Formal analysis, Funding acquisition, Project administration, Writing – original draft, Writing – review & editing. **José V. García-Pérez:** Conceptualization, Methodology, Formal analysis, Supervision, Writing – original draft, Writing – review & editing.

Declaration of competing interest

None.

Data availability

Data will be made available on request.

Acknowledgements

This study was supported by the grant, PID2019-106148RRC42, funded by MCIN/AEI/10.13039/501100011033, the PhD grant of Gentil A. Collazos-Escobar, PRE2020-092255, funded by the State Training Subprogram of the State Plan for Scientific and Technical Research and Innovation 2017–2020 and the European Social Fund, and the funding for open access charge: Universitat Politècnica de València.

List of abbreviations

a_w	water activity
X_e	equilibrium moisture content (% d.b.)
T	absolute temperature (K)
h	hue angle
C_r	chroma or saturation
F_r	fracture force (N)
X_m	monolayer moisture content (% d.b.)
C	Guggenheim-Anderson-de Boer (GAB) model parameter
K	Guggenheim-Anderson-de Boer model parameter
H_m	monolayer sorption heat (kJ mol^{-1})
H_n	multilayer sorption heat (kJ mol^{-1})
K_0	preexponential (GAB) parameter
C_0	preexponential (GAB) parameter
R	universal gas constant of water vapor (8.31447 × 10^{-3} kJ

	mol^{-1} K^{-1})
L_r	latent heat of water vaporization (kJ mol^{-1})
Y_{exp}	experimental response (a_w/X_e)
Y_{pred}	predicted response (a_w/X_e)
N	number of experimental data
S_A	adsorption surface area (m^2 g^{-1} d.b.)
π	spreading pressure (J m^{-2})
M_w	molecular weight of water (kg mol^{-1})
N_0	Avogadro number (6×10^{23} molecules mol^{-1})
A_m	area for a water molecule (1.06×10^{-19} m^2 $molecule^{-1}$)
k	Boltzmann's constant (1.380×10^{-23}J K^{-1})
r_c	critical pore size (nm)
t	adsorbed water multilayer thickness (nm)
r_p	effective pore size (nm)
σ	surface tension of water (N m^{-1})
V_m	molar of adsorbate in a bulk liquid state (m^3 mol^{-1})
ΔG	Gibbs free energy for water adsorption (kJ mol^{-1})
ΔH_{diff}	net isosteric heat of adsorption (kJ mol^{-1})
ΔS_{diff}	differential adsorption entropy (kJ mol^{-1} K^{-1})
T_β	isokinetic temperature (K)
ΔG_β	Gibbs free energy at the isokinetic temperature (kJ mol^{-1})
T_{hm}	harmonic temperature (K)
n_t	total number of isotherms
ΔH_{int}	net integral heat of adsorption (kJ mol^{-1})
ΔS_{int}	integral entropy (kJ mol^{-1} K^{-1})
a_w^*	geometric water activity
b_i	empirical model parameters
MSE	mean square error (residual units)
R^2	coefficient of determination (%)
R^2_{adj}	adjusted coefficient of determination (%)
MRE	mean relative error (%)
M	number of model parameters

References

Acuff, J. C., Dickson, J. S., Farber, J. M., Grasso-Kelley, E. M., Hedberg, C., Lee, A., & Zhu, M.-J. (2023). Practice and progress: Updates on outbreaks, advances in research, and processing Technologies for low-moisture food safety. *Journal of Food Protection, 86*(1), Article 100018. https://doi.org/10.1016/j.jfp.2022.11.010

Al-Muhtaseb, A. H., Hararah, M. A., Megahey, E. K., McMinn, W. A. M., & Magee, T. R. A. (2010). Moisture adsorption isotherms of microwave-baked Madeira cake. *LWT - Food Science and Technology, 43*(7), 1042–1049. https://doi.org/10.1016/j.lwt.2010.01.003

Alyousef, H., ben Yahia, M., & Aouaini, F. (2020). Statistical physics modeling of water vapor adsorption isotherm into kernels of dates: Experiments, microscopic interpretation and thermodynamic functions evaluation. *Arabian Journal of Chemistry, 13*(3), 4691–4702. https://doi.org/10.1016/j.arabjc.2019.11.004

Anastopoulos, I., Karamesouti, M., Mitropoulos, A. C., & Kyzas, G. Z. (2017). A review for coffee adsorbents. *Journal of Molecular Liquids, 229*, 555–565. https://doi.org/10.1016/j.molliq.2016.12.096

Aouaini, F., Knani, S., Yahia, M. B., & Lamine, A. B. (2015). Statistical physics studies of multilayer adsorption isotherm in food materials and pore size distribution. *Physica A, 432*, 373–390. https://doi.org/10.1016/j.physa.2015.03.052

Arslan-Tontul, S. (2020). Moisture sorption isotherm, isosteric heat and adsorption surface area of whole chia seeds. *Lwt, 119*(October 2019), Article 108859. https://doi.org/10.1016/j.lwt.2019.108859

Baskaran, S., & Sathiavelu, M. (2020). Application of Attenuated Total Reflection - fourier Transform Infrared spectroscopy to characterize the degradation of littered multilayer food packaging plastics. *Vibrational Spectroscopy, 109*. https://doi.org/10.1016/j.vibspec.2020.103105

Beygelzimer, A., Kakadet, S., Langford, J., Arya, S., Mount, D., & Li, S. (2023). *FNN: Fast nearest neighbor search algorithms and applications*. R package version 1.1.3.2 https://CRAN.R-project.org/package=FNN.

Bon, J., Váquiro, H. A., & Mulet, A. (2012). Modeling sorption isotherms and isosteric heat of sorption of mango pulp C.V Tommy Atkins. *Biotecnología en el sector agropecuario y agroindustrial, 10*(2), 34–43.

Cano-higuita, D. M., Villa-vélez, H. A., Telis-romero, J., Alexander, H., Regina, V., & Telis, N. (2013). Food and bioproducts processing influence of alternative drying aids on water sorption of spray dried mango mix powders : A thermodynamic approach. *Food and Bioproducts Processing, 93*(June), 19–28. https://doi.org/10.1016/j.fbp.2013.10.005

Carter, B. P., Galloway, M. T., Campbell, G. S., Carter, A. H., Carter, B. P., & Carter, A. H. (2015). The critical water activity from dynamic dewpoint isotherms as an indicator of pre-mix powder stability above and below the critical water activity and examined. *Journal of Food Measurement and Characterization*. https://doi.org/10.1007/s11694-015-9256-1

de Cássia Sousa Mendes, D., Asquieri, E. R., Batista, R. D., de Morais, C. C., Ramirez Ascheri, D. P., de Macêdo, I. Y. L., & de Souza Gil, E. (2021). Microencapsulation of jabuticaba extracts (Myrciaria cauliflora): Evaluation of their bioactive and thermal properties in cassava starch biscuits. *Lebensmittel-Wissenschaft und -Technologie, 137*. https://doi.org/10.1016/j.lwt.2020.110460

Červenka, L., Stępień, A., Frühbauerová, M., Velichová, H., & Witczak, M. (2019). Thermodynamic properties and glass transition temperature of roasted and unroasted carob (Ceratonia siliqua L.) powder. *Food Chemistry, 300*(July), Article 125208. https://doi.org/10.1016/j.foodchem.2019.125208

Cheng, X., Zhang, M., & Adhikari, B. (2020). Moisture adsorption in water caltrop (Trapa bispinosaRoxb.) pericarps: Thermodynamic properties and glass transition. *Journal of Food Process Engineering*. https://doi.org/10.1111/jfpe.13442. *March*, 1–11.

Collazos-Escobar, G. A., Gutiérrez-Guzmán, N., Váquiro-Herrera, H. A., & Amorocho-Cruz, C. M. (2020). Water dynamics adsorption properties of dried and roasted cocoa beans (theobroma cacao L.). *International Journal of Food Properties, 23*(1). https://doi.org/10.1080/10942912.2020.1732408

Collazos-Escobar, G. A., Gutiérrez-Guzmán, N., Váquiro-Herrera, H. A., Bon, J., & Garcia-Perez, J. V. (2022). Thermodynamic analysis and modeling of water vapor adsorption isotherms of roasted specialty coffee (Coffee arabica L. cv. Colombia). *Lebensmittel-Wissenschaft und -Technologie, 160*. https://doi.org/10.1016/j.lwt.2022.113335

Cristina Duarte Marques, R., Resende Oliveira, É., Silva Mendes Coutinho, G., Emannuele Chaves Ribeiro, A., Souza Teixeira, C., Soares Soares Júnior, M., & Caliari, M. (2020). Modeling sorption properties of maize by-products obtained using the Dynamic Dewpoint Isotherm (DDI) method. *Food Bioscience, 38*(July). https://doi.org/10.1016/j.fbio.2020.100738

Durak, T., & Depciuch, J. (2020). Effect of plant sample preparation and measuring methods on ATR-FTIR spectra results. *Environmental and Experimental Botany, 169*. https://doi.org/10.1016/j.envexpbot.2019.103915

Fritsch, S., Guenther, F., & Wright, M. (2019). *neuralnet: Training of neural Networks*. R package version 1.44.2 https://CRAN.R-project.org/package=neuralnet.

Galla, N. R., Pamidighantam, P. R., Karakala, B., Gurusiddaiah, M. R., & Akula, S. (2017). Nutritional, textural and sensory quality of biscuits supplemented with spinach (Spinacia oleracea L.). *International Journal of Gastronomy and Food Science, 7*, 20–26. https://doi.org/10.1016/j.ijgfs.2016.12.003

Hanson, B. (2023). *ChemoSpec: Exploratory chemometrics for spectroscopy*. R package version 6.1.9 https://CRAN.R-project.org/package=ChemoSpec.

Herman, C., Spreutels, L., Turomzsa, N., Konagano, E. M., & Haut, B. (2018). Convective drying of fermented Amazonian cocoa beans (Theobroma cacao var. Forasteiro). Experiments and mathematical modeling. *Food and Bioproducts Processing, 108*, 81–94. https://doi.org/10.1016/j.fbp.2018.01.002

Hidar, N., Ouhammou, M., Idlimam, A., Jaouad, A., Bouchdoug, M., Lamharrar, A., Kouhila, M., & Mahrouz, M. (2018). Investigation of water adsorption and thermodynamic properties of stevia powder. *Journal of Food Measurement and Characterization, 12*(4), 2615–2625. https://doi.org/10.1007/s11694-018-9879-0

Iaccheri, E., Laghi, L., Cevoli, C., Berardinelli, A., Ragni, L., Romani, S., & Rocculi, P. (2015). Different analytical approaches for the study of water features in green and roasted coffee beans. *Journal of Food Engineering, 146*, 28–35. https://doi.org/10.1016/j.jfoodeng.2014.08.016

Kademi, H. I., Saad, F. T., Ulusoy, B. H., Baba, I. A., & Hecer, C. (2019). Mathematical model for aflatoxins risk mitigation in food. *Journal of Food Engineering, 263*, 25–29. https://doi.org/10.1016/j.jfoodeng.2019.05.030

Karatzoglou, A., Smola, A., & Hornik, K. (2023). *kernlab: Kernel-Based machine learning lab. R package versión 0* (pp. 9–32). https://CRAN.R-project.org/package=kernlab.

Kulchan, R., Boonsupthip, W., & Suppakul, P. (2010). Shelf life prediction of packaged cassava-flour-based baked product by using empirical models and activation energy for water vapor permeability of polyolefin films. *Journal of Food Engineering, 100*(3), 461–467. https://doi.org/10.1016/j.jfoodeng.2010.04.031

Liaw, A., & Wiener, M. (2002). Classification and regression by randomForest. *R News, 2*(3), 18–22. https://CRAN.R-project.org/doc/Rnews/.

McMinn, W. A. M., McKee, D. J., & Magee, T. R. A. (2007). Moisture adsorption behaviour of oatmeal biscuit and oat flakes. *Journal of Food Engineering, 79*(2), 481–493. https://doi.org/10.1016/j.jfoodeng.2006.02.009

Mendez-Montealvo, G., Velazquez, G., Fonseca-Florido, H. A., Morales-Sanchez, E., & Soler, A. (2022). Insights on the acid hydrolysis of achira (Canna edulis) starch: Crystalline and double-helical structure changes impacting functionality. *Lebensmittel-Wissenschaft und -Technologie, 153*. https://doi.org/10.1016/j.lwt.2021.112509

Monte, M. L., Moreno, M. L., Senna, J., Arrieche, L. S., & Pinto, L. A. A. (2018). Moisture sorption isotherms of chitosan-glycerol films: Thermodynamic properties and microstructure. *Food Bioscience, 22*(February), 170–177. https://doi.org/10.1016/j.fbio.2018.02.004

Otchere, D. A. (2023). Fundamental error in tree-based machine learning model selection for reservoir characterisation. *Energy Geoscience*. https://doi.org/10.1016/j.engeos.2023.100229

Ramírez, M., Gutiérrez, N., & Cortés, E. (2016). Evolución de atributos de calidad en bizcocho de achira (Canna edulis Ker.) del Huila. *Agronomía Colombiana, 34*, 728–730. https://doi.org/10.15446/agron.colomb.v34n1supl.57783

Robertson, G. L., & Lee, D. S. (2021). Comparison of linear and GAB isotherms for estimating the shelf life of low moisture foods packaged in plastic films. *Journal of Food Engineering, 291*. https://doi.org/10.1016/j.jfoodeng.2020.110317

Romani, S., Rocculi, P., Tappi, S., & Dalla Rosa, M. (2016). Moisture adsorption behaviour of biscuit during storage investigated by using a new Dynamic Dewpoint

method. *Food Chemistry, 195*, 97–103. https://doi.org/10.1016/j.foodchem.2015.06.114

Sairamya, N. J., Susmitha, L., Thomas George, S., & Subathra, M. S. P. (2019). Hybrid approach for classification of electroencephalographic signals using time-frequency images with wavelets and texture features. In *Intelligent data analysis for biomedical applications: Challenges and solutions* (pp. 253–273). Elsevier. https://doi.org/10.1016/B978-0-12-815553-0.00013-6.

Sanchez-Jimenez, V., Collazos-Escobar, G. A., González-Mohino, A., Alvarez-Arenas, T. E., Benedito, J., & Garcia-Perez, J. V. (2023). Non-invasive monitoring of potato drying by means of air-coupled ultrasound. *Food Control.* , Article 109653. https://doi.org/10.1016/j.foodcont.2023.109653

Sánchez-Torres, E. A., Abril, B., Benedito, J., Bon, J., & García-Pérez, J. V. (2021). Water desorption isotherms of pork liver and thermodynamic properties. *Lwt, 149*. https://doi.org/10.1016/j.lwt.2021.111857

Scatigno, C., & Festa, G. (2022). FTIR coupled with machine learning to unveil spectroscopic benchmarks in the Italian EVOO. *International Journal of Food Science and Technology, 57*(7), 4156–4162. https://doi.org/10.1111/ijfs.15735

Schmidt, J. S., & Won, L. J. (2012). Comparison between water vapor Sorption isotherms obtained using the new Dynamic dewpoint isotherm method and those obtained using the standard saturated salt slurry method. *International Journal of Food Properties, 15*, 236–248. https://doi.org/10.1080/10942911003778014, 2012.

Schmitt, J., Bönig, J., Borggräfe, T., Beitinger, G., & Deuse, J. (2020). Predictive model-based quality inspection using machine learning and edge cloud computing. *Advanced Engineering Informatics, 45*. https://doi.org/10.1016/j.aei.2020.101101

Silva, E. K., Fernandes, R. V. D. B., Borges, S. V., Botrel, D. A., & Queiroz, F. (2014). Water adsorption in rosemary essential oil microparticles: Kinetics, thermodynamics and storage conditions. *Journal of Food Engineering, 140*, 39–45. https://doi.org/10.1016/j.jfoodeng.2014.05.003

Silva, K. S., Polachini, T. C., Luna-Flores, M., Luna-Solano, G., Resende, O., & Telis-Romero, J. (2021). Sorption isotherms and thermodynamic properties of wheat malt under storage conditions. *Journal of Food Process Engineering*. https://doi.org/10.1111/jfpe.13784. *February*, 1–12.

Talens, C., Castro-Giraldez, M., & Fito, P. J. (2018). Effect of microwave power coupled with hot air drying on sorption isotherms and microstructure of orange peel. *Food and Bioprocess Technology, 11*(4), 723–734. https://doi.org/10.1007/s11947-017-2041-x

Tanui, C. K., Karanth, S., Njage, P. M. K., Meng, J., & Pradhan, A. K. (2022). Machine learning-based predictive modeling to identify genotypic traits associated with Salmonella enterica disease endpoints in isolates from ground chicken. *Lebensmittel-Wissenschaft und -Technologie, 154*. https://doi.org/10.1016/j.lwt.2021.112701

Tao, Y., Wu, Y., Yang, J., Jiang, N., Wang, Q., Chu, D., Han, Y., & Zhou, J. (2018). Thermodynamic sorption properties , water plasticizing effect and particle characteristics of blueberry powders produced from juices , fruits and pomaces. *Powder Technology, 323*, 208–218. https://doi.org/10.1016/j.powtec.2017.09.033

Torgo, L. (2016). *Data Mining with R, learning with case studies* (2nd ed.). Chapman and Hall/CRC. URL http://ltorgo.github.io/DMwR2.

Tripetch, P., & Borompichaichartkul, C. (2019). Effect of packaging materials and storage time on changes of colour, phenolic content, chlorogenic acid and antioxidant activity in arabica green coffee beans (Coffea arabica L. cv. Catimor). *Journal of Stored Products Research, 84*, Article 101510. https://doi.org/10.1016/j.jspr.2019.101510

Üçüncüoğlu, D., & Küçük, V. A. (2019). A multivariate data approach for FTIR-ATR monitoring of virgin olive oils: Lipid structure during autoxidation. *OCL - Oilseeds and Fats, Crops and Lipids, 26*. https://doi.org/10.1051/ocl/2019043

Velásquez, S., Franco, A. P., Peña, N., Bohórquez, J. C., & Gutierrez, N. (2021). Effect of coffee cherry maturity on the performance of the drying process of the bean: Sorption isotherms and dielectric spectroscopy. *Food Control, 123*, 1–8. https://doi.org/10.1016/j.foodcont.2020.107692

Viganó, J., Azuara, E., Telis, V. R. N., Beristain, C. I., Jiménez, M., & Telis-Romero, J. (2012). Role of enthalpy and entropy in moisture sorption behavior of pineapple pulp powder produced by different drying methods. *Thermochimica Acta, 528*, 63–71. https://doi.org/10.1016/j.tca.2011.11.011

Wang, Z., Chockchaisawasdee, S., Ashton, J., Fang, Z., & Stathopoulos, C. E. (2021). Study on glass transition of whole-grain wheat biscuit using Dynamic Vapor Sorption, Differential Scanning Calorimetry, and texture and color analysis. *Lebensmittel-Wissenschaft und -Technologie, 150*. https://doi.org/10.1016/j.lwt.2021.111969

Ying, D. Y., Hlaing, M. M., Lerisson, J., Pitts, K., Cheng, L., Sanguansri, L., & Augustin, M. A. (2017). Physical properties and FTIR analysis of rice-oat flour and maize-oat flour based extruded food products containing olive pomace. *Food Research International, 100*, 665–673. https://doi.org/10.1016/j.foodres.2017.07.062

Yogendrarajah, P., Samapundo, S., Devlieghere, F., De Saeger, S., & De Meulenaer, B. (2015). Moisture sorption isotherms and thermodynamic properties of whole black peppercorns (Piper nigrum L). *LWT - Food Science and Technology, 64*(1), 177–188. https://doi.org/10.1016/j.lwt.2015.05.045